Journal of Magnetism and Magnetic Materials 469 (2019) 443–449

Contents lists available at ScienceDirect

Journal of Magnetism and Magnetic Materials

journal homepage: www.elsevier.com/locate/jmmm

Research articles

Synthesis of iron oxide nanorods for enhanced magnetic hyperthermia

Aleksey Nikitin[a,b,*], Maxim Khramtsov[a], Anastasiia Garanina[a,b], Pavel Mogilnikov[a], Natalya Sviridenkova[a], Igor Shchetinin[a], Alexander Savchenko[a], Maxim Abakumov[a,c], Alexander Majouga[b,d]

[a] National University of Science and Technology "MISIS", Leninskiy Prospect 4, 119991 Moscow, Russian Federation
[b] Department of Chemistry, Lomonosov Moscow State University, Leninskiye Gory 1-3, GSP-1, 119991 Moscow, Russian Federation
[c] Pirogov Russian National Research Medical University, Ostrovityanova 1, 117997 Moscow, Russian Federation
[d] Dmitry Mendeleev University of Chemical Technology of Russia, Miusskaya Sq. 9, Moscow, 125047 Russian Federation

ARTICLE INFO

Keywords:
Nanoparticles
Iron oxide
Nanorods
Hyperthermia

ABSTRACT

Magnetic hyperthermia is one of the most effective methods for treatment of cancer. In this work we discuss synthesis of magnetic iron oxide nanorods (IONRds) and their application for enhanced magnetic hyperthermia. By microwave irradiation the monodisperse water-soluble IONRds with clear morphology were obtained. Magnetic measurements showed that such IONRds have high value of coercivity (141 Oe). Moreover, hyperthermia experiments with synthesized samples were carried out. At the frequency and field strength of alternating magnetic field (AMF) f = 261 kHz H = 20 kA m^{-1} the specific absorption rate (SAR) and intrinsic loss power (ILP) values were equal to 147 W g^{-1} and 1.4 nHm^2 kg^{-1} respectively, which confirms the efficiency of synthesized nanorods in hyperthermia applications.

1. Introduction

Anisotropic magnetic nanoparticles are of particular interest for biomedical applications [1]. Previously it has been shown that such nanoparticles can be used in magnetic resonance imaging (MRI) as effective contrast agents [2–6] as well as in drug delivery [7].

In recent years, increased interest has been given to the development of magnetic nanoparticles for the treatment of tumors by hyperthermia [8,9]. Under the action of a high-frequency magnetic field, such nanoparticles produce a heat and lead to local damage and destruction of defective cells, while healthy cells remain intact.

The shape, size and efficiency of heating, characterized by the specific absorption rate (SAR) of magnetic nanoparticles are the key parameters that determine their suitability and effectiveness for hyperthermia. A number of authors investigated size-dependent heating of magnetic nanoparticles [10,11]. Numerous experimental data on the SAR study for magnetic iron oxide nanoparticles with a magnetic core size ≤ 20 nm indicate the maximum efficiency of hyperthermia for 15 nm nanoparticles [12–14]. However, these data contradict the fact that some of the highest SAR values were obtained for iron oxide nanoparticles with a magnetic core size > 20 nm [15].

Moreover, it was shown that anisotropic nanoparticles are more preferable for hyperthermia than spherical one [8,16,17]. Recently Raja Das et al. demonstrated that the SAR of iron oxide nanostructures can be enhanced and tuned by altering their aspect ratio [18]. In this work a comparison between spherical, cubic and rod-like nanoparticles was carried out as a result of which it was found that the last one demonstrate the highest SAR value (862 W/g for AMF with frequency of 310 kHz and H = 300 Oe). Due to the high aspect ratio, magnetic nanorods have the high values of coercivity and produce a lot of heat in high frequency magnetic field, which can be effectively used in tumor hyperthermia. Additionally, it was shown that magnetic nanorods interaction with a lipid membrane can cause membrane deformation under the action of an AMF [19]. Thus, synthesis and physicochemical investigation of iron oxide nanorods for enhanced magnetic hyperthermia is very important task, requiring more detailed study.

2. Experimental section

2.1. Materials

Iron (III) chloride ($FeCl_3$; 97%, reagent grade), branched polyethylenimine (PEI; M_w = 25000), hydrazine hydrate (50–60%, reagent grade), NaOH (reagent grade), HCl (36%), HNO_3 (65%), ethanol (95%) and acetone (99%) were purchased from Sigma-Aldrich. All reagents were used without any further purification. 3-(4,5-dimethylthiazol-2-

* Corresponding author at: Department of Chemistry, Lomonosov Moscow State University, Leninskiye Gory 1-3, GSP-1, 119991 Moscow, Russian Federation.
E-mail address: nikitin.chemistry@mail.ru (A. Nikitin).

https://doi.org/10.1016/j.jmmm.2018.09.014
Received 24 June 2018; Received in revised form 4 September 2018; Accepted 4 September 2018
Available online 05 September 2018
0304-8853/

Table 1
The main parameters of the syntheses and the obtained results.

Sample	Concentration of hydrazine hydrate in final solution, mol/L	Number of irradiation cycles	Shape of nanoparticles	The average size of nanoparticles, nm	
				Length	Diameter
N-0	0	0	rod-like	21	4
N-1	0.052	3	rod-like	21	4
N-2	0.103	3	rod-like polyhedral plates	22 28	4
N-3	0.503	3	polyhedral plates	35	

yl)-5-(3-carboxymethoxyphenyl)-2-(4-sulfophenyl)–2H-tetrazolium (MTS) (CellTiter 96 AQueous Non-Radioactive Cell Proliferation Assay) was purchased from Promega, USA. Ultra-pure deionized Milli-Q water was obtained by Millipore Milli-Q Academic System.

2.2. β-FeOOH nanorods synthesis

β-FeOOH nanorods were obtained by hydrolysis of $FeCl_3$ water solution in the presence of brunched high-weight PEI [20]. Firstly, 4 mL of PEI were dissolved in 200 mL of deionized water in 250 mL round-bottom flask, after that 5.08 g of $FeCl_3$ were added to the obtained solution. The mixture was heated to 80 °C under magnetic stirring for 2 h. After cooling the mixture to room temperature the pH was adjusted to 7.0 by 2 M NaOH. The precipitate was separated by centrifugation and washed several times with deionized water.

2.3. IONRds synthesis

β-FeOOH nanorods water solution with iron concentration [Fe] = 3 mg/mL were mixed with different amounts of hydrazine hydrate (Table 1). The mixture was placed in hermetic ampoule, which was then undergone by various number of microwave irradiation cycles (each cycle included heating solution to 100 °C, sustaining for 30 s and cooling down to 35 °C). Microwave synthesis was performed in Anton Paar – Monowave 300 microwave synthesis reactor in 30 mL vials. The final product was separated from solution by centrifugation and washed several times with deionized water.

2.4. Samples characterization

2.4.1. Transmission electron microscopy (TEM) investigations.

TEM images of synthesized samples were taken on JEOL JEM-1400 (120 kV) microscope. All samples were prepared by dropping water dispersion of synthesized samples onto a carbon-coated copper grid (300 mesh) and subsequently evaporating the solvent. The average diameter and size distribution were evaluated by using ImageJ software.

2.4.2. X-ray diffraction (XRD) analysis

XRD patterns were obtained using an X-ray power diffractometer Rigaku Ultima IV with Co Kα radiation at room temperature. The data were collected from 2θ = 20 to 140° at a scan rate 0,1° per step and 3 s per point.

2.4.3. Magnetic measurements

M − H hysteresis loops (from −30 to 30 kOe, 300 K) were obtained on «Quantum Design» Physical Property Measurement System (PPMS) equipped with vibration magnetometric device (VSM) with 2 mm amplitude of oscillations, 40 Hz frequency.

2.4.4. Thermogravimetric analysis

Thermogravimetric curves were recorded on synchronous thermogravimetric analyzer Netzsch STA 449 F3. In a typical procedure 5 mg of samples were heated in corundum crucibles under argon flow in temperature range 50–800 °C with a heating rate of 10 °C/min.

2.4.5. Fourier transform infrared (FTIR) spectroscopy

FTIR spectra of samples were registered by means of a Nicolet 380 instrument (Thermo Scientific, USA), in KBr, in the range 400–4000 cm^{-1}. Infrared spectra were obtained by the KBr pellet method. In this method, the solid sample is finely pulverized with pure, dry KBr, the mixture is pressed in a hydraulic press to form a transparent pellet, and the spectrum of the pellet is measured.

2.4.6. Dynamic light scattering (DLS) analysis and ζ-potential measurements

DLS analysis and ζ-potential measurements were performed on Zetasiser Nano ZS device. The iron concentration in each sample was 1 mg/mL.

2.4.7. Magnetic hyperthermia

Hyperthermia experiments were performed in an alternating magnetic field generator Nanomaterials TOR ULTRA HT with biologically reasonable field parameters: strength of magnetic field H = 20 kA m^{-1} and frequency f = 261400 Hz. 150 μL of each sample were tested in a range of different concentrations, which were determined using a standard ferrozine-based assay protocol [21].

2.4.8. Cell culture

4 T1 mouse breast cancer cells were purchased from the American Type Culture Collection (ATCC, Manassas, VA, USA). Cells were cultured in RPMI-1640 medium (Gibco) supplemented with 10% fetal bovine serum (FBS) (Gibco) and 2 mM L-glutamine (Gibco) at 37 °C in a humidified incubator supplied with 5% CO_2.

2.4.9. Hyperthermia in vitro experiments

Cells were seeded in the wells of Stripwell 96 well plates (Corning) at concentration of 10 000 cells per well. Automatic cell counter EVE was used to count the cells. After 2 days, culture medium from the cells was replaced by 150 μL of nanoparticles solution in sorbitol. Obtained samples were exposure to high-frequency alternating magnetic field (AMF) for 15–20 min. Following parameters of AMF were applied – f = 261–393 kHz, H = 20 kA m^{-1} – to keep constant temperature. A magnetic field was created in an AMF generator TOR UltraHT. The temperature was measured by thermal imager Seek Thermal. Cells, incubated in full culture medium, sorbitol and nanoparticles in sorbitol at 37 °C in the incubator, were used as controls.

2.4.10. MTS assay

After hyperthermia, the medium with nanoparticles from each well was replaced by 120 μL of new culture medium/MTS reagent solution at a rate of 20 μL MTS reagent per 100 μL culture medium. Cells were incubated with MTS for 4 h at 37 °C in darkness. After this wells were placed on the permanent magnet in order to remove nanoparticles from solution, and 80 μL of the obtained solution were carefully replaced in new 96-well plate. The absorbance of the solution was measured at 490 nm using Thermo Scientific Multiskan GO spectrometer.

2.5. Statistical analysis

The percentage of live cells in the MTS-assay was represented as mean ± SD (for four repeats in each experiment). Percentage of live cells, cultivated in full culture medium in incubator, was taken as 100%. Plotting and calculation of the standard deviation value were made using Microsoft Excel software. *P* value was calculated using one-way ANOVA calculator. *P* values < 0.01 were considered significant.

3. Results and discussion

3.1. Synthesis of nanorods

Previously several approaches to synthesize iron oxide nanorods were described [20,22]. In these works, the resulting iron oxide nanorods were hydrophobic due to the usage of oleylamine or hexadeclamine and further surface functionalization in order to get a stable colloidal water solution was needed. We suggest a faster method including hydrolysis of iron (III) salt in the PEI presence as previously described [20] and the following reduction of obtained nonmagnetic precursor (β-FeOOH) by hydrazine hydrate under microwave irradiation. Hydrazine hydrate acts as an electron donor for the reduction of Fe^{3+} to Fe^{2+} according to Eq. (1):

$$12\beta\text{–FeOOH(s)} + N_2H_4(aq) \rightarrow 4Fe_3O_4(s) + 8H_2O + N_2(g) \quad (1)$$

Earlier, the attempts to describe the mechanism and kinetics of the process of akaganeite reduction to magnetite under the action of hydrazine hydrate were carried out [23]. According to this investigation the mechanism of such reduction can be described as Eqs. (2)–(4):

$$\beta\text{–FeOOH(s)} + H_2O \leftrightarrow Fe(III)(aq) + 3OH^- \quad (2)$$

$$Fe(III)(aq) + \frac{1}{4}N_2H_4 \rightarrow Fe(II) + \frac{1}{4}N_2 + H^+ \quad (3)$$

$$Fe(II)(aq) + 2\beta\text{–FeOOH(s)} \rightarrow Fe_3O_4(s) + 2H^+ \quad (4)$$

Microwave-assisted chemical reactions are now well-established practice to produce nanoparticles and various organic substances [24]. However, microwave synthesis of nanoparticles requires the selection of certain parameters, which is a laborious task. We developed and optimized the scheme for producing magnetic IONRds. The synthesis scheme gives several opportunities to vary the parameters in order to get the IONRds with the desired size, morphology and SAR values. Firstly, the amount of PEI can directly affect the size of nanorods [20]. In our work we used 2 mL of PEI to produce β-FeOOH nanorods with length 21 nm and diameter 4 nm (Fig. 1). Secondly, the number of microwave irradiation cycles varied from 1 to 3. Finally, the hydrazine hydrate concentration in final solution varied from 0.052 mol/L to 0.503 mol/L (Table 1).

3.2. Characterization of samples by TEM

To show the influence of hydrazine hydrate as well as the amounts of microwave irradiation cycles on the final shape of the samples the transmission electron microscopy was performed. As a result, a number of images of samples was obtained (Fig. 1). It can be seen that β-FeOOH precursor (N-0) and sample N-1 have the clear rod-like morphology. The samples N-2 and N-3 represent the mixture of nanorods and polyhedron nanoparticles. All histograms of nanoparticles size distribution are presented in Fig. S1. The average length and diameter of the precursor N-0 are 21 and 4 nm respectively (aspect ratio is 5.25).

One cycle of microwave irradiation of the precursor N-0 in the concentration range of hydrazine hydrate from 0.052 to 0.503 mol/L led to the formation of nanorods that did not have magnetic properties. Two cycles of microwave irradiation of N-0 at hydrazine hydrate concentration 0.052 mol/L resulted in obtaining magnetic nanorods, however, the study of the sample phase composition showed the presence of goethite (α-FeOOH) and akaganeite (β-FeOOH) in nanorods structure (Fig. S2). The increase in the concentration of hydrazine hydrate led to the loss of the rod-like shape of nanoparticles (Fig. S3). Finally, we investigated the influence of three microwave irradiation cycles of N-0 on the final shape and structure of obtained nanoparticles. As a result, after the reduction of the precursor at the concentration of hydrazine hydrate 0.052 mol/L using three microwave irradiation cycles we preserved rod-like shape and size of nanoparticles (N-1) and obtained pure magnetite phase composition (Fig. 1, Fig. 2). The average length and diameter of N-1 are 21 and 4 nm respectively (aspect ratio is 5.25). A further increase in the concentration of the reducing agent led to a gradual loss of the rod-like shape of the nanoparticles. At the concentration of hydrazine hydrate 0.103 mol/L (N-2) a large number of polyhedron nanoparticles with average size 28 nm were formed. The concentration of hydrazine hydrate 0.503 mol/L (N-3) led to formation of iron oxide nanoparticles with various shapes and average size 35 nm. Thus, using such scheme of reduction we preserved the aspect ratio = 5.25 of nanorods in comparison with other works [20,25] in which the precursor loses the rod-like shape after reduction.

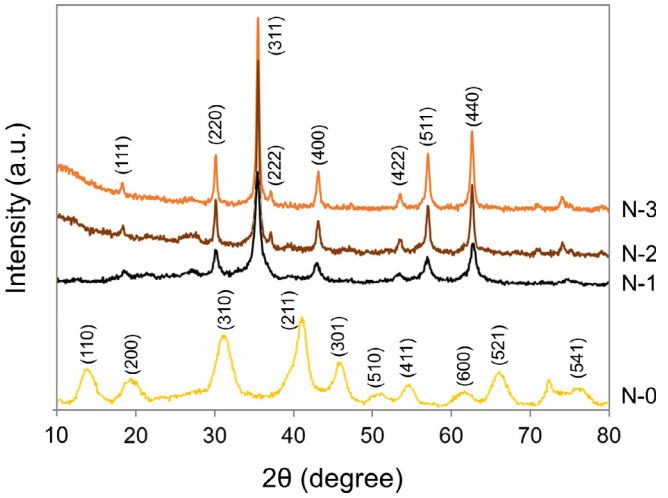

Fig. 2. XRD patterns of synthesized samples with the indexation of the Bragg peaks.

3.3. Characterization of samples by XRD

The X-ray diffraction patterns of synthesized samples are shown in Fig. 2. The position and relative intensity of the diffraction peaks for precursor (N-0) can be indexed to pure akaganeite β-FeOOH (a = 10.535 Å, c = 3.030 Å, ICDD 34–1266). After reduction of

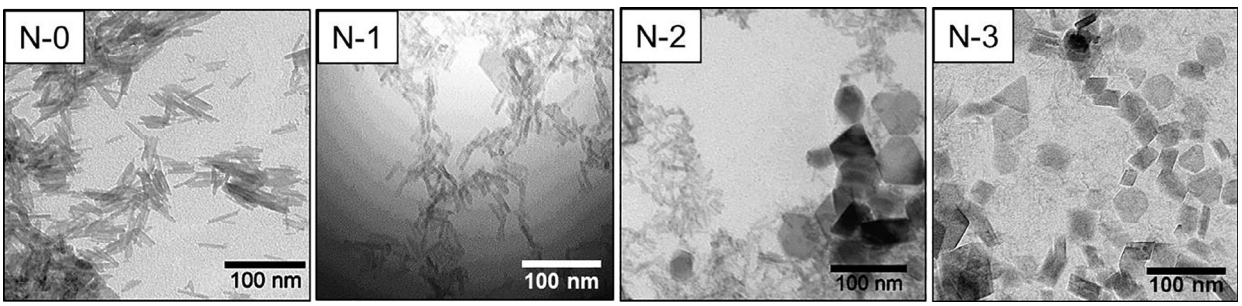

Fig. 1. TEM images of synthesized samples.

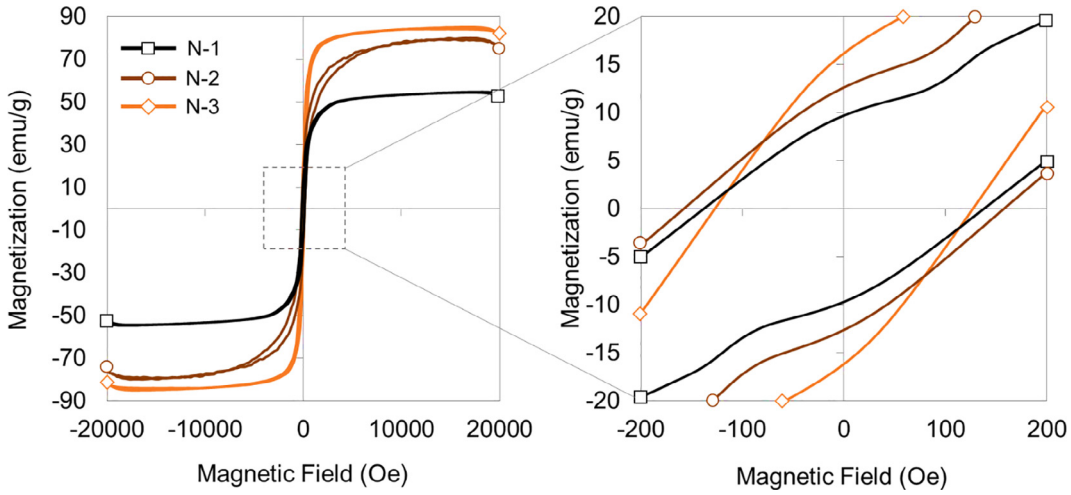

Fig. 3. Room temperature magnetic curves of samples.

precursor in the presence of hydrazine hydrate by microwave oven the new diffraction peaks are observed. The XRD spectra of samples N-1, N-2 and N-3 can be attributed to magnetite Fe_3O_4 (a = 8.396 Å, ICDD no. 19–0629) or maghemite γ-Fe_2O_3 (a = 8.346 Å, ICDD 39–1346) patterns. The XRD characteristics of the obtained samples are presented in Table S1.

3.4. Magnetic properties of samples

The M − H loops of synthesized samples are shown in Fig. 3. Magnetic hysteresis measurements were normalized to magnetite content determined using TGA (Fig. S4). At the temperatures of 50–200 °C the weight loss is related to removal of the physically adsorbed water on the surface of nanoparticles. Also it is known that the degradation of inorganic and organic molecules occurs in the range from 100 to 500 °C. Weight reduction at the range above 500 °C is most likely due to the magnetite phase transformation processes [26]. Especially for PEI coat it has been observed that it decomposed at the temperatures of 200–400 °C [27,28]. For all three samples it can be seen from obtained TGA curves that the main weight losses occur up to 400 °C and further changes in the mass of the samples are insignificant (Fig. S4). In Fig. 3 it can be seen that the saturation magnetization values M_s increase to 85.1 emu/g with increasing average particle size. The main magnetic parameters of samples are presented in Table 2. The high values of coercivity prove ferromagnetic nature of synthesized samples.

In contrast to Mohapatra J. et al. [20] where M_s = 50 emu/g was obtained for IONRds with length 30 nm, in our work we observed the similar value (54.4 emu/g) for 21 nm nanorods

N-1. Furthermore, the authors noted the superparamagnetic behavior of 30–70 nm Fe_3O_4 nanorods, which contradicts the results obtained for 21 nm N-1, which has a coercivity of 141 Oe. However, the magnetic measurements data for nanorods N-1 correlate with earlier works [29] where the value of M_s = 58 emu/g was obtained for γ-Fe_2O_3 nanorods with length 30 ± 9.7 nm and diameter 5.7 ± 1.8 nm (aspect ratio = 5.26). Thus, the synthesized samples demonstrate high coercivity values, which is one of the important magnetic characteristics determining the possibility of using nanoparticles for hyperthermia.

Table 2
Magnetic parameters of samples.

Sample	Magnetic properties		
	Saturation magnetization, M_s (emu/g)	Remanent magnetization, M_r (emu/g)	Coercivity, H_c (Oe)
N-1	54.4	9.1	141
N-2	79.9	12.1	163
N-3	85.1	15.7	130

3.5. Characterization of samples by FTIR

Fig. 4 presents the FTIR spectra of PEI and synthesized nanorods N-0 and N-1. The band at around 3275 cm^{-1} corresponds to the vibration of the N–H bond in PEI molecules. The peaks at 2932 cm^{-1} and 2809 cm^{-1} are consistent with the stretching vibration of C–H and the peak at 1457 cm^{-1} corresponds to the C–H scissoring bending vibration. The peaks at 1107 cm^{-1} and 1043 cm^{-1} are consistent with the stretching vibration of C–N bond. It can be clearly seen the C-N stretching vibration in FTIR spectra of N-0 and N-1. Moreover, the peaks at 2924 cm^{-1} and 2853 cm^{-1} corresponds to the C–H stretching vibration. The band at 625 cm^{-1} is assigned to the stretching mode of the Fe-O bond. These facts prove the successfully immobilizing PEI on the surface of nanoparticles.

3.6. Magnetic hyperthermia

Magnetic nanoparticles hyperthermia experiments were performed at 261 kHz under an AMF with field strength 20 kA m^{-1} using the device TOR ULTRA HT designed by NanoMaterials® (Tambov, Russia). Each measurement cycle included a heating and a cooling stage. The heating of the nanoparticles water solutions was continued until a linear dependence of the heating rate was obtained in order to calculate

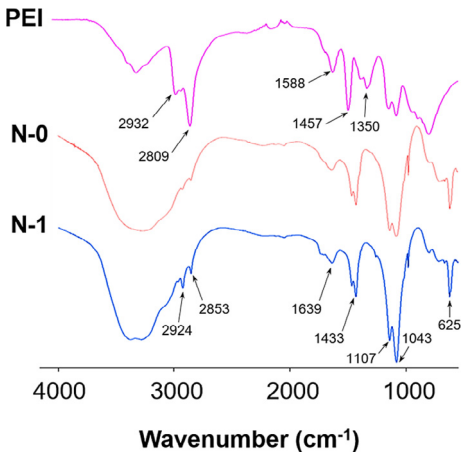

Fig. 4. FTIR spectra of PEI and synthesized samples.

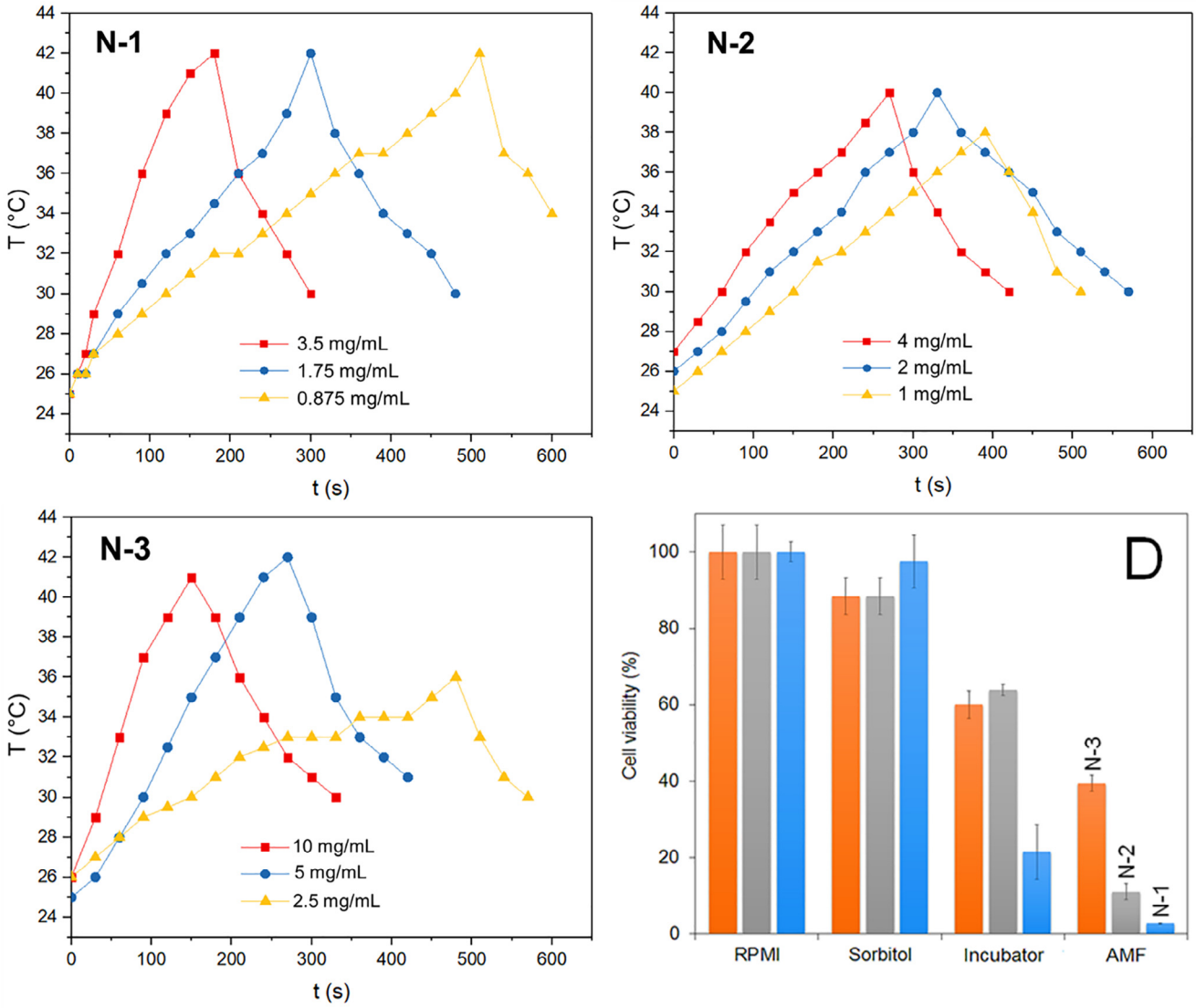

Fig. 5. Localized heating of synthesized nanoparticles in an AMF: N-1(A), N-2 (B), N-3 (C) and histograms of cell (4 T1) viability in the absence of AMF and after magnetic hyperthermia in the presence of synthesized nanoparticles (D).

Table 3
Specific absorption rate and intrinsic loss power values for synthesized nanoparticles.

sample	H, kA m^{-1}	f (kHz)	SAR (W g^{-1})	ILP (nHm^2 kg^{-1})
N-1	20	261	147	1.4
N-2	20	261	87	0.8
N-3	20	261	56	0.5

the SAR, after that the heating was stopped. Thus, 150 μL of nanoparticles water solution with different iron concentrations was placed into the cuvette and the temperature was measured by thermal imager Seek Thermal. As a result, for each sample (N-1, N-2 and N-3) three heating–cooling curves corresponding to certain iron concentrations were obtained (Fig. 5). The heating efficiency of samples is quantified by the specific absorption rate (SAR) determined from the power absorption per unit mass of magnetic material (in W/g) following a standardized procedure to estimate solely the magnetic heating contribution by using the following formula [30]:

$$SAR = c_p \frac{\Delta T}{\Delta t} \frac{m_f}{m_{MNPs}}$$

where c_p is the volume specific heat capacity of the sample (4.179 J/(g °C) for water at 25 °C), m_f the mass dispersion (0.15 g), m_{MNPs} is the iron oxide mass diluted in the dispersion and $\Delta T/\Delta t$ is the average value of the maximal slope at initial time after switching on the magnetic field H. SAR values for each sample were calculated as an average for three different nanoparticles concentrations, which are presented in Fig. 5. In order to normalize SAR values and compare the obtained results on the nanoparticles heating efficiency with previously published ones, the value of the intrinsic loss power (ILP) was calculated [30] (Table 3):

$$ILP = \frac{SLP}{H^2 f}$$

where H is the strength of the magnetic field and f is the frequency.

In Table 3 it can be seen that the N-1 has the highest value of SAR (147 W g^{-1}). For samples N-2 and N-3 significant heating with analogous amounts of nanoparticles and field parameters was not observed, and therefore large amounts of nanoparticles were required to produce heating–cooling curves (Fig. 5A-C). The increase of SAR values with the increasing magnetic core size was noted earlier [31]. However, in our case the polydispersity of nanoparticles increases, which leads to a decrease the heat generation rate and this fact is in good agreement

with previously published work [11]. Hydrodynamic size and PDI values for samples N-1, N-2 and N-3 are presented in table (Fig. S5). Dynamic light scattering (DLS) measurements show that hydrodynamic size and polydispersity index (PDI) of synthesized nanoparticles increases from N-1 sample to N-3. TEM images also show that from sample N-1 to N-3 overall size of crystals is increased. Moreover, because DLS measurements are based on assumption that all nanoparticles are spherical shape overall anisotropy of synthesized nanoparticles will lead to increase in PDI values. For all samples N-1, N-2 and N-3 ζ-potential measurements show the positive charge of nanoparticles surface equal to 36.1, 41.6, 44.5 mV respectively. Due to use of as stabilizing agent PEI we believe that main contribution to ζ-potential is made amino groups of PEI molecules which are positively charged in water solution. The obtained value of ILP = 1.4 for N-1 is sufficiently high for hyperthermia application and can be compared with ILP values for previously synthesized nanoparticles [32]. Das R. and colleagues synthesized magnetite nanorods by hydrothermal method and measured SAR values [18]. For the nanorods with length 41 nm and diameter 7 nm (aspect ratio = 5.8) the SAR value in water was ~ 170 W/g (H = 300 Oe, f = 302 kHz). It corresponds to the ILP value 0.99. In our work we obtained almost one and a half times more value of ILP for N-1. Thus, under using biologically reasonable field parameters of AMF we obtained high value of SAR for iron oxide nanorods, which can be effectively used in tumor hyperthermia.

Moreover, this fact was confirmed by in vitro analysis of nanoparticles-mediated hyperthermia on 4 T1 cell line. After placing in a high-frequency magnetic field (261 kHz, 20 kA m^{-1}), the cells were heated to a temperature of 39 °C after 2 min by N-1 (3.5 mg/mL). After this cells were heated at temperature 43–45 °C during 13 min. Such hyperthermia caused 95% of cell death compared to cells, incubated with sorbitol during this time ($p < 0.01$) (Fig. 5D-blue columns). However, the viability of cells cultivated with N-1 in CO_2 incubator during the experiment decreased by 75.5% in comparison with sorbitol sample ($p < 0.01$) that can be due to the fact that the rod-like nanoparticles were found to produce much higher cytotoxic responses than spherical, cubic or octahedron nanoparticles [33,34]. In the case of N-2 (3.5 mg/mL) the temperature 39 °C was reached only after 7 min exposure to AMF with parameters 261 kHz, 20 kA m^{-1}. After this cells were maintained at a temperature of 43–45 °C during 13 min. It led to death of 77% of cells in comparison with cells in sorbitol ($p < 0.01$). Also sorbitol by itself caused death of 12% of cell in comparison with cells in culture medium during this time of the experiment (Fig. 5D-grey columns). N-3 (3.5 mg/mL) led to 39 °C heating of cells only after 9 min of exposure to magnetic field with parameters 261 kHz, 20 kA m^{-1}. The maximum achieved temperature was 41 °C. Cells were maintained at it during 13 min. Such hyperthermia caused death of only 59% of cell compared to cells in sorbitol ($p < 0.01$) (Fig. 5D-orange columns). It must be noted, that both N-2 and N-3 were less toxic for cells: these samples resulted in 25–28% of dead cells in population relative to cells in sorbitol while N-1 exposure to cells resulted in 75.5% of dead cells as it was discussed above. Thus, we demonstrated that nanoparticles-mediated magnetic hyperthermia causes very effective tumor cell death. The sample N-1 which is presented rod-like nanoparticles allows to achieve optimum heating in less time and at lower parameters of AMF than N-2 and N-3.

4. Conclusions

In this work, we developed and optimized the method for producing iron oxide nanorods by microwave irradiation of akaganeite precursor. The structure and the magnetic properties of samples were investigated. Magnetic measurements showed the high coercivity for synthesized nanorods with length 21 nm and diameter 4 nm (aspect ratio 5.25). Hyperthermia experiments revealed the effective heating of nanorods in a high-frequency magnetic field under biologically reasonable field parameters (f = 261 kHz, H = 20 kA m^{-1}). In vitro studies showed the lower survival of breast cancer cells (4 T1) after hyperthermia in the presence of synthesized nanoparticles. Thus, synthesized nanorods N-1 caused 95% of cell death after hyperthermia, while samples N-2 and N-3 representing a mixture of nanorods and polyhedron nanoparticles resulted in 77 and 59% cell death respectively.

5. Notes

The authors declare no competing financial interest.

6. Author contributions

This manuscript was written through contribution of all authors. All authors have given approval to the final version of the manuscript.

Acknowledgment

The reported study was funded by RFBR according to the research project no. 17-00-00442 and Ministry of Education and Science of the Russian Federation, in the framework of the Increase Competitiveness Program of NUST “MISIS” (Grants No. K2-2018-008).

Appendix A. Supplementary data

Supplementary data associated with this article can be found, in the online version, at https://doi.org/10.1016/j.jmmm.2018.09.014.

References

[1] D. Lisjak, A. Mertelj, Anisotropic magnetic nanoparticles: a review of their properties, syntheses and potential applications, Progr. Mater. Sci. 95 (2018) 286–328.
[2] S. Nath, C. Kaittanis, V. Ramachandran, N.S. Dalal, J.M. Perez, Synthesis, magnetic characterization, and sensing applications of novel dextran-coated iron oxide nanorods, Chem. Mater. 21 (2009) 1761–1767.
[3] A. Nikitin, et al., Synthesis, characterization and MRI application of magnetite water-soluble cubic nanoparticles, J. Magn. Magn. Mater. 441 (2017) 6–13.
[4] Z. Zhou, et al., Anisotropic shaped iron oxide nanostructures: controlled synthesis and proton relaxation shortening effects, Chem. Mater. 27 (2015) 3505–3515.
[5] J. Mohapatra, A. Mitra, H. Tyagi, D. Bahadur, M. Aslam, Iron oxide nanorods as high-performance magnetic resonance imaging contrast agents, Nanoscale 7 (2015) 9174–9184.
[6] A. Orza, H. Wu, Y. Xu, Q. Lu, H. Mao, One-step facile synthesis of highly magnetic and surface functionalized iron oxide nanorods for biomarker-targeted applications, ACS Appl. Mater. Interfaces 9 (2017) 20719–20727.
[7] P. Yu, et al., Folic acid-conjugated iron oxide porous nanorods loaded with doxorubicin for targeted drug delivery, Colloid Surf. B Biointerfaces 120 (2014) 142–151.
[8] Z. Nemati, et al., Enhanced magnetic hyperthermia in iron oxide nano-octopods: size and anisotropy effects, J. Phys. Chem. C 120 (2016) 8370–8379.
[9] J. Kolosnjaj-Tabi, et al., Heat-generating iron oxide nanocubes: Subtle ‘destructurators’ of the tumoral microenvironment, ACS Nano 8 (2014) 4268–4283.
[10] S. Tong, C.A. Quinto, L. Zhang, P. Mohindra, G. Bao, Size-dependent heating of magnetic iron oxide nanoparticles, ACS Nano 11 (2017) 6808–6816.
[11] M. Gonzales-Weimuller, M. Zeisberger, K.M. Krishnan, Size-dependant heating rates of iron oxide nanoparticles for magnetic fluid hyperthermia, J. Magn. Magn. Mater. 321 (2009) 1947–1950.
[12] R. Chen, M.G. Christiansen, P. Anikeeva, Maximizing hysteretic losses in magnetic ferrite nanoparticles via model-driven synthesis and materials optimization, ACS Nano 7 (2013) 8990–9000.
[13] L. Lartigue, et al., Water-dispersible sugar-coated iron oxide nanoparticles. An evaluation of their relaxometric and magnetic hyperthermia properties, J. Am. Chem. Soc. 133 (2011) 10459–10472.
[14] M. Levy, et al., Correlating magneto-structural properties to hyperthermia performance of highly monodisperse iron oxide nanoparticles prepared by a seeded-growth route, Chem. Mater. 23 (2011) 4170–4180.
[15] P. Guardia, et al., One pot synthesis of monodisperse water soluble iron oxide nanocrystals with high values of the specific absorption rate, J. Mater. Chem. B 2 (2014) 4426.
[16] C. Martinez-Boubeta, et al., Learning from nature to improve the heat generation of iron-oxide nanoparticles for magnetic hyperthermia applications, Sci. Rep. 3 (2013).
[17] M. Cho, et al., Assembly of iron oxide nanocubes for enhanced cancer hyperthermia and magnetic resonance imaging, Nanomaterials 7 (2017) 72.
[18] R. Das, et al., Tunable high aspect ratio iron oxide nanorods for enhanced hyperthermia, J. Phys. Chem. C 120 (2016) 10086–10093.
[19] Y.I. Golovin, et al., Towards nanomedicines of the future: Remote magneto-mechanical actuation of nanomedicines by alternating magnetic fields, J. Controll.

Release 219 (2015) 43–60.
[20] J. Mohapatra, A. Mitra, H. Tyagi, D. Bahadur, M. Aslam, Iron oxide nanorods as high-performance magnetic resonance imaging contrast agents, Nanoscale 7 (2015).
[21] J. Riemer, H.H. Hoepken, H. Czerwinska, S.R. Robinson, R. Dringen, Colorimetric ferrozine-based assay for the quantitation of iron in cultured cells, Anal. Biochem. 331 (2004) 370–375.
[22] H. Sun, et al., Solvothermal synthesis of tunable electroactive magnetite nanorods by controlling the side reaction, J. Phys. Chem. C 116 (2012) 5476–5481.
[23] M.A. Blesa, M. Mijalchik, M. Villegas, G. Rigotti, Transformation of akaganeite into magnetite in aqueous hydrazine suspensions, React. Solids (1986), https://doi.org/10.1016/0168-7336(86)80066-3.
[24] M.B. Gawande, S.N. Shelke, R. Zboril, R.S. Varma, Microwave-assisted chemistry: synthetic applications for rapid assembly of nanomaterials and organics, Acc. Chem. Res. 47 (2014) 1338–1348.
[25] S. Lentijo Mozo, E. Zuddas, A. Casu, A. Falqui, Synthesizing iron oxide nanostructures: the polyethylenenemine (PEI) role, Crystals 7 (2017) 22.
[26] K. Yang, H. Peng, Y. Wen, N. Li, Re-examination of characteristic FTIR spectrum of secondary layer in bilayer oleic acid-coated Fe3O4nanoparticles, Appl. Surf. Sci. (2010), https://doi.org/10.1016/j.apsusc.2009.11.079.
[27] C.Q. Peng, Y.S. Thio, R.A. Gerhardt, Enhancing the layer-by-layer assembly of indium tin oxide thin films by using polyethyleneimine, J. Phys. Chem. C (2010), https://doi.org/10.1021/jp101722u.
[28] F. Wang, P. Liu, T. Nie, H. Wei, Z. Cui, Characterization of a polyamine microsphere and its adsorption for protein, Int. J. Mol. Sci. (2013), https://doi.org/10.3390/ijms14010017.
[29] C.-M. Lee, H.-J. Jeong, S.T. Lim, M.-H. Sohn, D.W. Kim, Synthesis of iron oxide nanoparticles with control over shape using imidazolium-based ionic liquids, ACS Appl. Mater. Interfaces 2 (2010) 756–759.
[30] M. Kallumadil, et al., Suitability of commercial colloids for magnetic hyperthermia, J. Magn. Magn. Mater. 321 (2009) 1509–1513.
[31] A. Jordan, T. Rheinländer, N. Waldöfner, R. Scholz, Increase of the specific absorption rate (SAR) by magnetic fractionation of magnetic fluids, J. Nanoparticle Res. 5 (2003) 597–600.
[32] C. Blanco-Andujar, et al., Design of iron oxide-based nanoparticles for MRI and magnetic hyperthermia, Nanomedicine 11 (2016) 1889–1910.
[33] V. Forest, et al., Impact of cerium oxide nanoparticles shape on their in vitro cellular toxicity, Toxicol. Vitr. (2017), https://doi.org/10.1016/j.tiv.2016.09.022.
[34] J.H. Lee, et al., Rod-shaped iron oxide nanoparticles are more toxic than sphere-shaped nanoparticles to murine macrophage cells, Environ. Toxicol. Chem. (2014), https://doi.org/10.1002/etc.2735.